

Topological magnons in Kitaev magnets with finite Dzyaloshinskii-Moriya interaction at high field

Kangkang Li^{1,*}

¹*Department of Physics, Zhejiang Normal University, Jinhua, 321004, China*

There have been intensive studies on Kitaev materials for the sake of the realization of exotic states such as quantum spin liquid and topological orders. In realistic materials, the Kitaev interaction may coexist with the Dzyaloshinskii-Moriya interaction (DMI), and it is a challenge to distinguish their magnitudes separately. Here, we study the topological magnon excitations and related thermal Hall conductivity of kagome magnet exhibiting Heisenberg, Kitaev and DM interactions exposed to a magnetic field. In a strong magnetic field perpendicular to the plane of the lattice ([111] direction) that bring the system into the fully polarized paramagnetic phase, we find that the magnon bands carry nontrivial Chern numbers in the full region of the phase diagram. Furthermore, there are phase transitions relate two topological phases with opposite Chern numbers, which lead to the sign changes of the thermal Hall conductivity. In the phase with negative thermal conductivity, the Kitaev interaction is relatively large and the width of the phase increases with the strength of DMI. Hence the study here will contribute to the understanding of related compounds.

I. INTRODUCTION

In recent years, quantum materials with bond-dependent anisotropic Kitaev spin interactions have been the subject of much experimental and theoretical studies, because there are frustrations from the competing exchange couplings coexisting with the geometric frustration of the underlying lattices, which may lead to unusual magnetic orders as well as gapped and gapless spin liquids with fractional excitations¹⁻⁸. However, the Kitaev interaction is often accompanied by the Dzyaloshinskii-Moriya interaction (DMI)^{9,10} in realistic materials, and it is a challenge to distinguish their magnitudes separately^{11,12}.

The Kitaev interaction also shows its exotic properties in magnonic side, for instance, it can realize topological magnon bands in various lattices such as honeycomb lattice¹²⁻¹⁵ and kagome lattice¹⁶. However, the effect of the Kitaev interaction can be generally similar to that of the DMI, which can also induce topological magnons and has been already studied in lots of experimental and theoretical works¹⁷⁻²⁵. In some cases, the spin wave spectrum of the Heisenberg-Kitaev model can even reduce to that of the Heisenberg model with DMI, and then hosts the same topological property¹⁵. Therefore, the same magnon bands and topological property can be generated either by Kitaev interaction, DMI, or their combination. Fortunately, it was shown that one can distinguish whether a system is Kitaev interaction or DMI dominated by further investigating the magnonic transport properties, for example, in honeycomb Kitaev magnet^{11,12}.

In this work, we study the topological magnon excitations and related thermal Hall conductivity of kagome magnet exhibiting Heisenberg, Kitaev and DM interactions exposed to a magnetic field. It is well known that the magnon bands of kagome ferromagnet with DMI carry nonzero Chern numbers²⁰. On the other hand, the kagome magnet with Kitaev interaction, whose ground state is canted ferromagnetic order^{26,27}, also hosts topo-

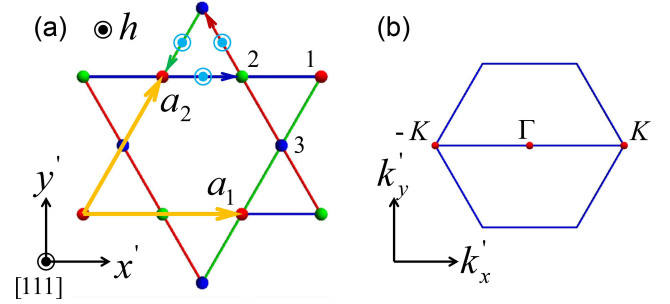


Figure 1. (a) The structure of the kagome lattice. There are three spins reside in a primitive cell, which are denoted by red, green and blue sites. Red, green and blue bonds between NN sites (i, j) carry three distinct Kitaev couplings $S_i^x S_j^x$, $S_i^y S_j^y$ and $S_i^z S_j^z$, respectively. Meanwhile, there are isotropic Heisenberg couplings in all the NN bonds. The arrows in a triangle denote the coupling directions whose DM vectors are in the [111] direction. The field is also applied in the [111] direction. The kagome lattice sits on the (111) plane, and we define a new 2D frame $x'y'$ on the kagome lattice with basis vectors $\mathbf{a}_1 = (1, 0)$ and $\mathbf{a}_2 = (1, \sqrt{3})/2$. (b) The first Brillouin zone of the kagome lattice.

logical magnon excitations¹⁶. Hence, one may wonder what would happen when there are DMI and Kitaev interaction in kagome magnet simultaneously. Since the Kitaev interaction does not support ferromagnetic order^{26,27}, we apply a magnetic field perpendicular to the plane of the lattice ([111] direction), which is strong enough to bring the system into fully polarized paramagnetic phase¹⁵. We find that the magnon bands carry nontrivial Chern numbers in the full region of the phase diagram. Furthermore, there are phase transitions relate two topological phases with opposite Chern numbers, which lead to the sign changes of the thermal Hall conductivity. In the phase with negative thermal conductivity, the Kitaev interaction is relatively large and the width of the phase increases with the strength of DMI.

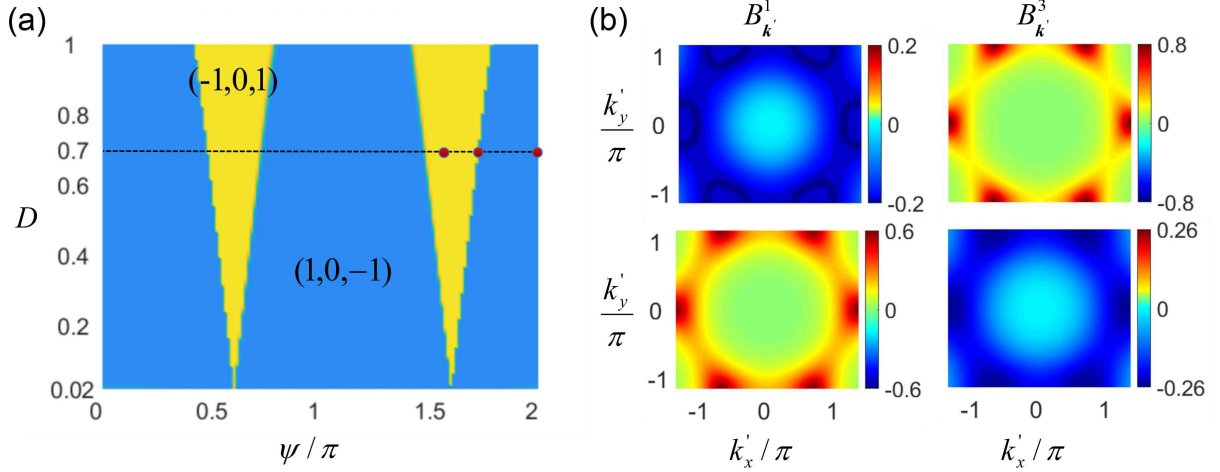


Figure 2. (a) The topological phase diagram of our model as a function of ψ and D . The topological phases are characterized by the Chern numbers of magnon bands, and the phase diagram is filled by two phases $(1, 0, -1)$ and $(-1, 0, 1)$. The three red points on the dashed line with $D = 0.7$ reside in phase $(-1, 0, 1)$ with $\psi = 1.57\pi$, at phase boundary with $\psi = 1.726\pi$ and in phase $(1, 0, -1)$ with $\psi = 2\pi$, respectively. (b) The Berry curvatures of the first and third magnon bands for $\psi = 1.57\pi$ (top panel) and $\psi = 2\pi$ (bottom panel) with $D = 0.7$.

Thus the study here will contribute to the understanding of related compounds.

This paper is organized as follows. In section II, we introduce the model and related methods. In section III, we discuss the topological magnons. In section IV, we present the thermal Hall conductivity with sign change. Finally, a summary is given in section V.

II. MODEL AND METHOD

We consider interacting spins reside on the kagome lattice as shown in Fig. 1(a). The model is described by the spin Hamiltonian

$$H = J \sum_{\langle ij \rangle} \mathbf{S}_i \cdot \mathbf{S}_j + K \sum_{\langle ij \rangle} S_i^{\gamma_{ij}} S_j^{\gamma_{ij}} + D \sum_{\langle ij \rangle} \nu_{ij} \hat{\mathbf{z}}' \cdot (\mathbf{S}_i \times \mathbf{S}_j) - h \sum_i \hat{\mathbf{z}}' \cdot \mathbf{S}_i, \quad (1)$$

where \mathbf{S}_i and \mathbf{S}_j are spin $S = 1/2$ spins reside on the nearest-neighbor (NN) lattice sites, and J and K denote the Heisenberg and Kitaev exchange couplings, respectively. The Cartesian components γ_{ij} equals x , y or z , depending on the bond type as shown in Fig. 1(a). We parameterize the Heisenberg and Kitaev terms by $J = \cos \psi$, $K = \sin \psi$, $\psi \in [0, 2\pi)$, with the energy unit $J^2 + K^2 = 1$. The NN DMI is represented by the third term, where $\hat{\mathbf{z}}'$ is the unit vector along [111] direction and $\nu_{ij} = \pm 1$ correspond to the anticlockwise and clockwise directions of the NN couplings in a triangle, respectively. In kagome magnet the Kitaev interaction does not support ferromagnetic order^{26,27}, hence we add the final term of Zeeman coupling to a applied magnetic field along the [111] direction, which is strong enough to

bring the system into fully polarized paramagnetic phase. We study a reasonable parameter range of $D \in [0, 1]$, and set $h = 10$ (in unit of S) all through the work to ensure the stability of the system.

Further, the Holstein-Primakoff (HP) transformation²⁸ is employed to rewrite the Hamiltonian in terms of magnon creation and annihilation operators a_i^\dagger and a_i . Under the linear spin wave approximation, we keep only the quadratic terms of the magnon operators. Then the Fourier transformation is performed to rewrite the Hamiltonian in momentum space with basis $\Psi_{\mathbf{k}'}^\dagger = (a_{1\mathbf{k}'}^\dagger, a_{2\mathbf{k}'}^\dagger, a_{3\mathbf{k}'}^\dagger, a_{1-\mathbf{k}'}, a_{2-\mathbf{k}'}, a_{3-\mathbf{k}'})$, and we get the magnon Hamiltonian matrix $h(\mathbf{k}')$ (see Appendix for details). Finally, the eigenvalues and eigenvectors are obtained by diagonalizing the dynamic matrix $I_- h(\mathbf{k}')$ with $I_- = [(I, 0), (0, -I)]$, I as the 3×3 identity matrix.

III. TOPOLOGICAL MAGNONS

We characterize the topological property of the model by the Chern number²⁹⁻³¹ of the n th magnon band

$$C_n = \frac{1}{2\pi} \int_{\text{BZ}} dk'_x dk'_y B_{k'_x k'_y}^n, \quad (2)$$

with the Berry curvature of the n th band

$$B_{k'_x k'_y}^n = i \sum_{n' \neq n} \frac{\langle \phi_n | \frac{\partial h(\mathbf{k}')}{\partial k'_x} | \phi_{n'} \rangle \langle \phi_{n'} | \frac{\partial h(\mathbf{k}')}{\partial k'_y} | \phi_n \rangle - (k'_x \leftrightarrow k'_y)}{(E_n - E_{n'})^2}, \quad (3)$$

where E_n and ϕ_n are the eigenvalue and eigenvector of the n th band respectively.

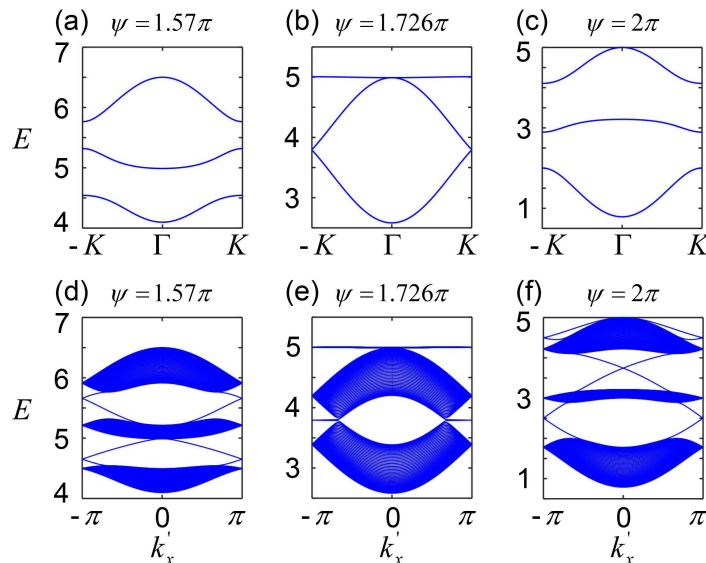


Figure 3. Top panel: magnon bands for (a) $\psi = 1.57\pi$, (b) $\psi = 1.726\pi$ and (c) $\psi = 2\pi$ all with $D = 0.7$, which are denoted in Fig. 2(a) as red points. For the point (b) sits at the phase boundary, the bands are gapless and there are Dirac points at the K points. Note that the top band in (b) has small dispersion. Bottom panel: the corresponding magnon bands in a strip geometry. There are in-gap edge modes in (d) and (f), and nondispersive edge modes connecting the Dirac points in (e).

The Heisenberg kagome magnet with only DMI or Kitaev interaction both host topological magnon excitations^{16,20}. The similar effects on magnon topology of the DMI and Kitaev interaction stem from their common origin, the spin-orbit coupling. However, due to their different formalisms of spin operators, there should also be competing effects. Here we find that the magnon bands of our model carry nontrivial Chern numbers in the full region of the phase diagram with the tuning of D and ψ , as shown in Fig. 2(a). We characterize the topological phase by (C_1, C_2, C_3) , and the phase diagram is filled by two phases $(1, 0, -1)$ and $(-1, 0, 1)$. Note that we only show the parameter range $D \in [0.02, 1]$ for the phase diagram, because there are complicated phases and phase transitions in the range $D \in [0, 0.02]$ and the magnitude of the related thermal conductivity is nearly zero, and these results are deviated from the theme of this paper.

One may note that, the two separated regions of the phase $(-1, 0, 1)$ have nearly the same shape, and they may can be related to each other by $\psi + \pi$. However, it is not exactly the case. The mapping $\psi \rightarrow \psi + \pi$ will take (J, K) to $(-J, -K)$ and the Zeeman coupling to the field will only give a energy shift of h for the whole spectrum, then if we have the eigenvalue of the n th band $E_{n,\psi,D}(\mathbf{k}') = \tilde{E}_n(\mathbf{k}') + h$, we must also have $E_{n,\psi+\pi,-D}(\mathbf{k}') = -\tilde{E}_n(\mathbf{k}') + h$. Hence we have the relation $(E_{n,\psi,D}(\mathbf{k}') + E_{n,\psi+\pi,-D}(\mathbf{k}'))/2 = h$, which means $E_{n,\psi,D}(\mathbf{k}')$ and $E_{n,\psi+\pi,-D}(\mathbf{k}')$ are mirror reflections of each other about the energy axis $E = h$. Thus the closing and re-opening of the band gap, which denotes a topological phase transition, is simultaneous for the bands $E_{n,\psi,D}(\mathbf{k}')$ and $E_{n,\psi+\pi,-D}(\mathbf{k}')$. Therefore, if we have

$E_{n,\psi+\pi,-D}(\mathbf{k}') = E_{n,\psi+\pi,D}(\mathbf{k}')$, the two separated regions of the phase $(-1, 0, 1)$ will be related to each other by $\psi + \pi$ and have exactly the same shape. However, we have checked that the sign change of D will affect the band shape slightly and break the simultaneity of the related phase transitions. Consequently, we only have similar but not the same shape of the two regions of the phase $(-1, 0, 1)$. Now the same Chern numbers of the two regions can also be understood easily. The mirror reflection about a constant energy axis does not change the Chern numbers of the bands, however, it will change the order of the bands. If the bands $E_{n,\psi,D}(\mathbf{k}')$ carry Chern numbers $(-1, 0, 1)$, then the mirror-reflected bands $E_{n,\psi+\pi,-D}(\mathbf{k}')$ will carry Chern numbers $(1, 0, -1)$. However, the sign change of D will change the sign of the Chern number of every band. Thus the bands $E_{n,\psi+\pi,D}(\mathbf{k}')$ will carry Chern numbers $(-1, 0, 1)$, which are the same with that of the bands $E_{n,\psi,D}(\mathbf{k}')$.

To gain a deeper insight of the topological property, we calculate the Berry curvatures of the magnon bands for $\psi = 1.57\pi$ and $\psi = 2\pi$ both with $D = 0.7$, which are in the phases $(-1, 0, 1)$ and $(1, 0, -1)$ respectively, as shown in Fig. 2(b). As for $\psi = 1.57\pi$ with $D = 0.7$, the Berry curvature of the first band is negative all over the Brillouin zone, and the integral of it gives Chern number -1 . While for the third band, its Berry curvature is always positive and gives Chern number 1. For $\psi = 2\pi$ with $D = 0.7$, the situation is reversed. The sign of the Berry curvature of the second band is momentum dependent for both cases, and they are not shown here.

In Fig. 3 we show the bulk magnon bands and their corresponding band structures in a strip geometry for $\psi = 1.57\pi$, $\psi = 1.726\pi$ and $\psi = 2\pi$ all with $D = 0.7$,

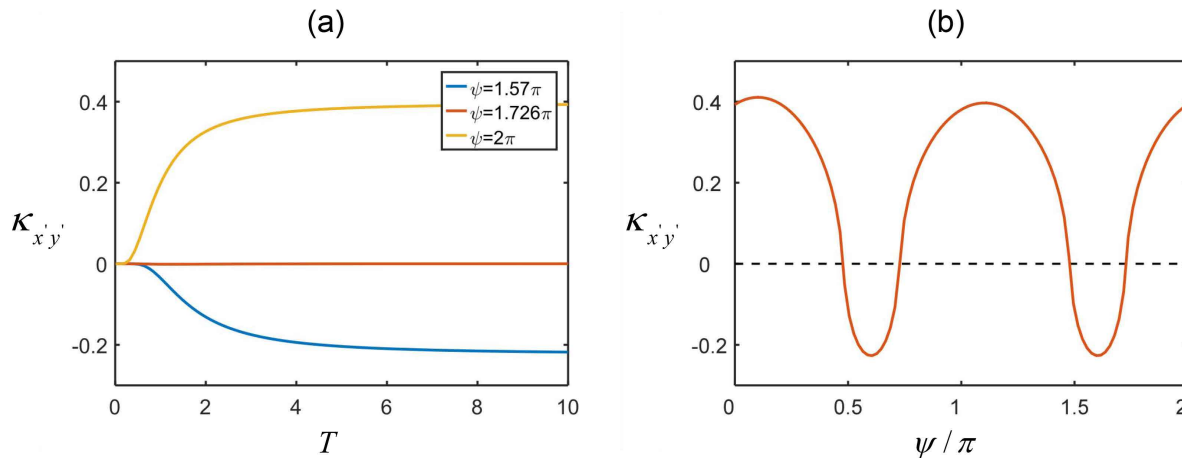


Figure 4. (a) The transverse thermal conductivity as function of temperature for $\psi = 1.57\pi$, $\psi = 1.726\pi$ and $\psi = 2\pi$ all with $D = 0.7$, which are denoted in Fig. 2(a) as red points. The thermal conductivity are always negative and positive for the phases $(-1, 0, 1)$ and $(1, 0, -1)$ respectively, and it is always zero for the phase boundary. (b) The transverse thermal conductivity as function of ψ with $D = 0.7$ and $T = 10$. There are sign changes at the phase boundaries. Here we set $\hbar = k_B = 1$.

which are denoted in Fig. 2(a) as red points. For the point sits at the phase boundary, the band structure is nearly the same with that of the Heisenberg kagome ferromagnet without DMI, the bands are gapless and there are Dirac points at the K points²⁰, except that here the top band has small dispersion. Due to the bulk-edge correspondence³², there are in-gap edge modes in the gapped band structures and nondispersive edge modes connecting the Dirac points.

IV. TRANSVERSE THERMAL HALL CONDUCTIVITY WITH SIGN CHANGE

The momentum independent sign structure of the Berry curvatures will lead to the sign change of the magnon thermal Hall conductivity, as we will show in this section. The transverse thermal Hall conductivity of magnon can be calculated as^{33–35}

$$\kappa_{x'y'} = \frac{k_B^2 T}{(2\pi)^2 \hbar} \sum_n \int_{\text{BZ}} c_2(\rho_n) B_{k'_x k'_y}^n dk'_x dk'_y, \quad (4)$$

with the sum running over the three bands and the integral is over the first Brillouin zone. $\rho_n = 1/(\exp(E_n/k_B T) - 1)$ is the Bose distribution with E_n as the n th eigenvalue. c_2 is given by

$$c_2(\rho_n) = (1 + \rho_n) \left(\ln \frac{1 + \rho_n}{\rho_n} \right)^2 - (\ln \rho_n)^2 - 2\text{Li}_2(-\rho_n), \quad (5)$$

where $\text{Li}_2(x)$ is the polylogarithm function of order 2.

As shown in Fig. 4(a) and 4(b), the thermal Hall conductivity are always negative and positive for the phases $(-1, 0, 1)$ and $(1, 0, -1)$ respectively, with the sign

changes happen at the phase boundaries, whose conductivity are always zero. The sign structure of the thermal conductivity stems from the sign structure of the Berry curvatures of the magnon bands. As for the phase $(-1, 0, 1)$, the negative and positive Berry curvatures of the first and third bands contribute to the Chern numbers -1 and 1 respectively. However, in the integral of the thermal conductivity, there is a weight $c_2(\rho_n) \geq 0$ which decreases monotonically with energy²⁵, thus the negative contribution from the first band is greater than the positive contribution from the third band, which leads to the negative conductivity. For the phase $(1, 0, -1)$, the situation is reversed and thus its conductivity is positive. We have checked that, the contributions from the second band are nearly zero for both phases. From the physical angle, the lowest magnon band will be thermally occupied maximally at low temperatures, and then dominate the thermal conductivity.

We note that, the phase $(-1, 0, 1)$ with negative thermal conductivity resides around $\psi = 0.6\pi$ and $\psi = 1.6\pi$ in the phase diagram, where the Kitaev interaction is relatively large with $|K| \approx 0.95$. Moreover, the width of the phase increases with the strength of DMI. These phenomena will be helpful to distinguish the relative strength of the isotropic Heisenberg interaction, the Kitaev interaction and the DMI.

V. SUMMARY

We have studied the topological magnon excitations and related thermal Hall conductivity in a kagome magnet exhibiting Heisenberg, Kitaev and DM interactions exposed to a magnetic field. We consider a strong enough field to bring the system into fully polarized paramagnetic phase. We find that the magnon bands carry non-

trivial Chern numbers in the full region of the phase diagram. Furthermore, there are phase transitions relate two topological phases with opposite Chern numbers, which lead to the sign changes of the thermal Hall conductivity. In the phase with negative thermal conductivity, the Kitaev interaction is relatively large and the width of the phase increases with the strength of DMI. Since the effects of magnon-magnon interactions are suppressed by the exchange scale divided by the applied field strength, the paramagnetic phase here is suitable for the exploration of related physics. Thus we believe that the study here will contribute to the understanding of related compounds.

ACKNOWLEDGEMENTS

We thank Changle Liu for helpful discussions. This work was supported by the National Natural Science Foundation of China (Grant NO. 12104407) and the Natural Science Foundation of Zhejiang Province (Grant NO. LQ20A040004).

APPENDIX: MAGNON HAMILTONIAN MATRIX

We denote the directions of spins $\mathbf{S}_{i=1,2,3}$ by their polar angles $\theta_{1,2,3}$ and azimuthal angles $\phi_{1,2,3}$ in the global frame. The HP transformation for a spin in its local frame reads

$$S_x^0 = \frac{\sqrt{2S}}{2}(a + a^\dagger), \quad (6)$$

$$S_y^0 = \frac{\sqrt{2S}}{2i}(a - a^\dagger), \quad (7)$$

$$S_z^0 = S - a^\dagger a, \quad (8)$$

where a^\dagger and a are the magnon creation and annihilation operators respectively, which obey the boson commutation rules. Then by multiplying a rotation matrix we get the HP transformation for spin \mathbf{S}_i in the global frame

$$\begin{pmatrix} S_{ix} \\ S_{iy} \\ S_{iz} \end{pmatrix} = \begin{pmatrix} \cos \theta_i \cos \phi_i & -\sin \phi_i & \sin \theta_i \cos \phi_i \\ \cos \theta_i \sin \phi_i & \cos \phi_i & \sin \theta_i \sin \phi_i \\ -\sin \theta_i & 0 & \cos \theta_i \end{pmatrix} \begin{pmatrix} S_{ix}^0 \\ S_{iy}^0 \\ S_{iz}^0 \end{pmatrix}. \quad (9)$$

Substituting $S_{i,x,y,z}$ into the Hamiltonian (1) and then do the Fourier transformation, we get the quadratic Hamiltonian in momentum space

$$H = \frac{1}{2} \sum_{\mathbf{k}'} \Psi_{\mathbf{k}'}^\dagger h(\mathbf{k}') \Psi_{\mathbf{k}'}, \quad (10)$$

where $\Psi_{\mathbf{k}'}^\dagger = (a_{1\mathbf{k}'}^\dagger, a_{2\mathbf{k}'}^\dagger, a_{3\mathbf{k}'}^\dagger, a_{1-\mathbf{k}'}, a_{2-\mathbf{k}'}, a_{3-\mathbf{k}'})$. The magnon Hamiltonian matrix is

$$h(\mathbf{k}') = \begin{pmatrix} A_{\mathbf{k}'} & B_{\mathbf{k}'}^\dagger \\ B_{\mathbf{k}'} & A_{\mathbf{k}'}^* \end{pmatrix} S, \quad (11)$$

with $A_{\mathbf{k}'}$ and $B_{\mathbf{k}'}$ 3×3 matrices. Their elements are as follows

$$A_{11} = -2J(c_z + e_z) - 2K(c_8 + e_7) - 2\frac{D}{\sqrt{3}}(c_D + e_D) + \frac{h}{\sqrt{3}}h_1, \quad (12)$$

$$A_{22} = -2J(c_z + d_z) - 2K(c_8 + d_6) - 2\frac{D}{\sqrt{3}}(c_D + d_D) + \frac{h}{\sqrt{3}}h_2, \quad (13)$$

$$A_{33} = -2J(d_z + e_z) - 2K(d_6 + e_7) - 2\frac{D}{\sqrt{3}}(d_D + e_D) + \frac{h}{\sqrt{3}}h_3, \quad (14)$$

$$A_{12} = [J(c_x + c_y - ic_{xy} + ic_{yx}) + Kc_3 + \frac{D}{\sqrt{3}}c_B^*] \cos \mathbf{k}' \cdot \boldsymbol{\delta}_1, \quad (15)$$

$$A_{21} = A_{12}^*, \quad (16)$$

$$A_{13} = [J(e_x + e_y + ie_{xy} - ie_{yx}) + K(e_2 + e_5 + ie_{10} - ie_{12}) + \frac{D}{\sqrt{3}}e_B] \cos \mathbf{k}' \cdot \boldsymbol{\delta}_3, \quad (17)$$

$$A_{31} = A_{13}^*, \quad (18)$$

$$A_{23} = [J(d_x + d_y - id_{xy} + id_{yx}) + K(d_1 + d_4 - id_9 + id_{11}) + \frac{D}{\sqrt{3}}d_B^*] \cos \mathbf{k}' \cdot \boldsymbol{\delta}_2, \quad (19)$$

$$A_{32} = A_{23}^*, \quad (20)$$

$$B_{12} = B_{21} = [J(c_x - c_y - ic_{xy} - ic_{yx}) + Kc_3 + \frac{D}{\sqrt{3}}c_A] \cos \mathbf{k}' \cdot \boldsymbol{\delta}_1, \quad (21)$$

$$B_{13} = B_{31} = [J(e_x - e_y - ie_{xy} - ie_{yx}) + K(e_2 - e_5 - ie_{10} - ie_{12}) + \frac{D}{\sqrt{3}}e_A] \cos \mathbf{k}' \cdot \boldsymbol{\delta}_3, \quad (22)$$

$$B_{23} = B_{32} = [J(d_x - d_y - id_{xy} - id_{yx}) + K(d_1 - d_4 - id_9 - id_{11}) + \frac{D}{\sqrt{3}}d_A] \cos \mathbf{k}' \cdot \boldsymbol{\delta}_2, \quad (23)$$

$$B_{11} = B_{22} = B_{33} = 0, \quad (24)$$

where

$$c_1 = \cos \theta_1 \cos \phi_1 \cos \theta_2 \cos \phi_2, \quad (25)$$

$$c_2 = \cos \theta_1 \sin \phi_1 \cos \theta_2 \sin \phi_2, \quad (26)$$

$$c_3 = \sin \theta_1 \sin \theta_2, \quad (27)$$

$$c_4 = \sin \phi_1 \sin \phi_2, \quad (28)$$

$$c_5 = \cos \phi_1 \cos \phi_2, \quad (29)$$

$$c_6 = \sin \theta_1 \cos \phi_1 \sin \theta_2 \cos \phi_2, \quad (30)$$

$$c_7 = \sin \theta_1 \sin \phi_1 \sin \theta_2 \sin \phi_2, \quad (31)$$

$$c_8 = \cos \theta_1 \cos \theta_2, \quad (32)$$

$$c_9 = -\cos \theta_1 \cos \phi_1 \sin \phi_2, \quad (33)$$

$$c_{10} = \cos \theta_1 \sin \phi_1 \cos \phi_2, \quad (34)$$

$$c_{11} = -\sin \phi_1 \cos \theta_2 \cos \phi_2, \quad (35)$$

$$c_{12} = \cos \phi_1 \cos \theta_2 \sin \phi_2, \quad (36)$$

$$c_x = c_1 + c_2 + c_3, \quad (37)$$

$$c_y = c_4 + c_5, \quad (38)$$

$$c_z = c_6 + c_7 + c_8, \quad (39)$$

$$c_{xy} = c_9 + c_{10}, \quad (40)$$

$$c_{yx} = c_{11} + c_{12}, \quad (41)$$

$$c_{13} = \sin \theta_1 \cos \theta_2 \sin \phi_2, \quad (42)$$

$$c_{14} = -\cos \theta_1 \sin \phi_1 \sin \theta_2, \quad (43)$$

$$c_{15} = \sin \theta_1 \sin \phi_1 \cos \theta_2, \quad (44)$$

$$c_{16} = -\cos \theta_1 \sin \theta_2 \sin \phi_2, \quad (45)$$

$$c_{17} = -\cos \phi_1 \sin \theta_2, \quad (46)$$

$$c_{18} = \sin \theta_1 \cos \phi_2, \quad (47)$$

$$c_{19} = \cos \theta_1 \cos \phi_1 \sin \theta_2, \quad (48)$$

$$c_{20} = -\sin \theta_1 \cos \theta_2 \cos \phi_2, \quad (49)$$

$$c_{21} = \cos \theta_1 \sin \theta_2 \cos \phi_2, \quad (50)$$

$$c_{22} = -\sin \theta_1 \cos \phi_1 \cos \theta_2, \quad (51)$$

$$c_{23} = \sin \theta_1 \sin \phi_2, \quad (52)$$

$$c_{24} = -\sin \phi_1 \sin \theta_2, \quad (53)$$

$$c_{25} = \cos \theta_1 \cos \phi_1 \cos \theta_2 \sin \phi_2, \quad (54)$$

$$c_{26} = -\cos \theta_1 \sin \phi_1 \cos \theta_2 \cos \phi_2, \quad (55)$$

$$c_{27} = \cos \phi_1 \sin \phi_2, \quad (56)$$

$$c_{28} = -\sin \phi_1 \cos \phi_2, \quad (57)$$

$$c_{29} = \sin \theta_1 \cos \phi_1 \sin \theta_2 \sin \phi_2, \quad (58)$$

$$c_{30} = -\sin \theta_1 \sin \phi_1 \sin \theta_2 \cos \phi_2, \quad (59)$$

$$c_{31} = \cos \theta_1 \cos \phi_1 \cos \phi_2, \quad (60)$$

$$c_{32} = \cos \theta_1 \sin \phi_1 \sin \phi_2, \quad (61)$$

$$c_{33} = -\sin \phi_1 \cos \theta_2 \sin \phi_2, \quad (62)$$

$$c_{34} = -\cos \phi_1 \cos \theta_2 \cos \phi_2, \quad (63)$$

$$c_{xxx} = c_{13} + c_{14}, \quad (64)$$

$$c_{xzz} = c_{15} + c_{16}, \quad (65)$$

$$c_{yxx} = c_{19} + c_{20}, \quad (66)$$

$$c_{yzz} = c_{21} + c_{22}, \quad (67)$$

$$c_{zxx} = c_{25} + c_{26}, \quad (68)$$

$$c_{zyy} = c_{27} + c_{28}, \quad (69)$$

$$c_{zzz} = c_{29} + c_{30}, \quad (70)$$

$$c_{zxy} = c_{31} + c_{32}, \quad (71)$$

$$c_{zyx} = c_{33} + c_{34}, \quad (72)$$

$$c_A = c_{xxx} + c_{yxx} + c_{zxx} - c_{zyy} - i(c_{17} + c_{24} + c_{zyx} + c_{18} + c_{23} + c_{zxy}), \quad (73)$$

$$c_B = c_{xxx} + c_{yxx} + c_{zxx} + c_{zyy} - i(c_{17} + c_{24} + c_{zyx} - c_{18} - c_{23} - c_{zxy}), \quad (74)$$

$$c_D = c_{xzz} + c_{yzz} + c_{zzz}, \quad (75)$$

and change the corresponding subscripts in $\theta_{1,2}$ and $\phi_{1,2}$ to $\theta_{2,3}$ and $\phi_{2,3}$, we get the corresponding expressions for d_i with

$$i = 1 - 34, x, y, z, xy, yx, xxx, xzz, yxx, yzz, zxx, zyy, zzz, zxy, zyx, A, B, D. \quad (76)$$

Similarly, change $\theta_{1,2}$ and $\phi_{1,2}$ to $\theta_{3,1}$ and $\phi_{3,1}$, we get the corresponding expressions for e_i . And we have

$$h_1 = \sin \theta_1 \cos \phi_1 + \sin \theta_1 \sin \phi_1 + \cos \theta_1, \quad (77)$$

$$h_2 = \sin \theta_2 \cos \phi_2 + \sin \theta_2 \sin \phi_2 + \cos \theta_2, \quad (78)$$

$$h_3 = \sin \theta_3 \cos \phi_3 + \sin \theta_3 \sin \phi_3 + \cos \theta_3, \quad (79)$$

Note that for the polarized phase here, we have $\theta_1 = \theta_2 = \theta_3 = \arctan \sqrt{2}$ and $\phi_1 = \phi_2 = \phi_3 = \pi/4$. The vectors $\delta_{1,2,3}$ are the NN vectors of the kagome lattice with $\delta_1 = (1/2, 0)$, $\delta_2 = (-1, \sqrt{3})/4$, $\delta_3 = (-1, -\sqrt{3})/4$, which are defined in the new 2D frame $x'y'$. Note that to get the eigenvalues and eigenvectors of bosonic quadratic Hamiltonian, we need to diagonalize the matrix $I_- h(\mathbf{k}')$ instead of $h(\mathbf{k}')$, where

$$I_- = \begin{pmatrix} I & 0 \\ 0 & -I \end{pmatrix}, \quad (80)$$

with I the 3×3 identity matrix .

- * physeeks@163.com
- 1 Ioannis Rousochatzakis, Johannes Reuther, Ronny Thomale, Stephan Rachel, and N. B. Perkins, “Phase diagram and quantum order by disorder in the kitaev $K_1 - K_2$ honeycomb magnet,” *Phys. Rev. X* **5**, 041035 (2015).
 - 2 Eric Kin-Ho Lee, Robert Schaffer, Subhro Bhattacharjee, and Yong Baek Kim, “Heisenberg-kitaev model on the hyperhoneycomb lattice,” *Phys. Rev. B* **89**, 045117 (2014).
 - 3 Joji Nasu, Masafumi Udagawa, and Yukitoshi Motome, “Vaporization of kitaev spin liquids,” *Phys. Rev. Lett.* **113**, 197205 (2014).
 - 4 T. Takayama, A. Kato, R. Dinnebier, J. Nuss, H. Kono, L. S. I. Veiga, G. Fabbris, D. Haskel, and H. Takagi, “Hyperhoneycomb iridate β - Li_2IrO_3 as a platform for kitaev magnetism,” *Phys. Rev. Lett.* **114**, 077202 (2015).
 - 5 Saeed S. Jahromi, Mehdi Kargarian, S. Farhad Masoudi, and Abdollah Langari, “Topological spin liquids in the ruby lattice with anisotropic kitaev interactions,” *Phys. Rev. B* **94**, 125145 (2016).
 - 6 Saeed S. Jahromi, Román Orús, Mehdi Kargarian, and Abdollah Langari, “Infinite projected entangled-pair state algorithm for ruby and triangle-honeycomb lattices,” *Phys. Rev. B* **97**, 115161 (2018).
 - 7 Masanori Kishimoto, Katsuhiko Morita, Yukihiko Matsubayashi, Shigetoshi Sota, Seiji Yunoki, and Takami Tohyama, “Ground state phase diagram of the kitaev-heisenberg model on a honeycomb-triangular lattice,” *Phys. Rev. B* **98**, 054411 (2018).
 - 8 Itamar Kimchi and Ashvin Vishwanath, “Kitaev-heisenberg models for iridates on the triangular, hyperkagome, kagome, fcc, and pyrochlore lattices,” *Phys. Rev. B* **89**, 014414 (2014).
 - 9 I. Dzyaloshinsky, “A thermodynamic theory of “weak” ferromagnetism of antiferromagnetics,” *Journal of Physics and Chemistry of Solids* **4**, 241–255 (1958).
 - 10 Tôru Moriya, “Anisotropic superexchange interaction and weak ferromagnetism,” *Phys. Rev.* **120**, 91–98 (1960).
 - 11 Yong Hao Gao, Ciarán Hickey, Tao Xiang, Simon Trebst, and Gang Chen, “Thermal hall signatures of non-kitaev spin liquids in honeycomb kitaev materials,” *Phys. Rev. Research* **1**, 013014 (2019).
 - 12 Li-Chuan Zhang, Fengfeng Zhu, Dongwook Go, Fabian R. Lux, Flaviano José dos Santos, Samir Lounis, Yixi Su, Stefan Blügel, and Yuriy Mokrousov, “Interplay of dzyaloshinskii-moriya and kitaev interactions for magnonic properties of heisenberg-kitaev honeycomb ferromagnets,” *Phys. Rev. B* **103**, 134414 (2021).
 - 13 Darshan G. Joshi, “Topological excitations in the ferromagnetic kitaev-heisenberg model,” *Phys. Rev. B* **98**, 060405 (2018).
 - 14 Li Ern Chern, Emily Z. Zhang, and Yong Baek Kim, “Sign structure of thermal hall conductivity and topological magnons for in-plane field polarized kitaev magnets,” *Phys. Rev. Lett.* **126**, 147201 (2021).
 - 15 P. A. McClarty, X.-Y. Dong, M. Gohlke, J. G. Rau, F. Pollmann, R. Moessner, and K. Penc, “Topological magnons in kitaev magnets at high fields,” *Phys. Rev. B* **98**, 060404 (2018).
 - 16 Kangkang Li, “Thermal hall conductivity with sign change in the heisenberg-kitaev kagome magnet,” [arXiv:2209.04133](https://arxiv.org/abs/2209.04133) (2022), [10.48550/arXiv.2209.04133](https://arxiv.org/abs/2209.04133).
 - 17 Hoshio Katsura, Naoto Nagaosa, and Patrick A. Lee, “Theory of the thermal hall effect in quantum magnets,” *Phys. Rev. Lett.* **104**, 066403 (2010).
 - 18 Y. Onose, T. Ideue, H. Katsura, Y. Shiomi, N. Nagaosa, and Y. Tokura, “Observation of the magnon hall effect,” *Science* **329**, 297–299 (2010), <https://www.science.org/doi/pdf/10.1126/science.1188260>.
 - 19 Max Hirschberger, Robin Chisnell, Young S. Lee, and N. P. Ong, “Thermal hall effect of spin excitations in a kagome magnet,” *Phys. Rev. Lett.* **115**, 106603 (2015).
 - 20 R. Chisnell, J. S. Helton, D. E. Freedman, D. K. Singh, R. I. Bewley, D. G. Nocera, and Y. S. Lee, “Topological magnon bands in a kagome lattice ferromagnet,” *Phys. Rev. Lett.* **115**, 147201 (2015).
 - 21 S A Owerre, “A first theoretical realization of honeycomb topological magnon insulator,” *Journal of Physics: Condensed Matter* **28**, 386001 (2016).
 - 22 Lifa Zhang, Jie Ren, Jian-Sheng Wang, and Baowen Li, “Topological magnon insulator in insulating ferromagnet,” *Phys. Rev. B* **87**, 144101 (2013).
 - 23 Kangkang Li, Chenyuan Li, Jiangping Hu, Yuan Li, and Chen Fang, “Dirac and nodal line magnons in three-dimensional antiferromagnets,” *Phys. Rev. Lett.* **119**, 247202 (2017).
 - 24 Kang-Kang Li and Jiang-Ping Hu, “Weyl and nodal ring magnons in three-dimensional honeycomb lattices,” *Chinese Physics Letters* **34**, 077501 (2017).
 - 25 Xiaodong Cao, Kai Chen, and Dahai He, “Magnon hall effect on the lieb lattice,” *Journal of Physics: Condensed Matter* **27**, 166003 (2015).
 - 26 Katsuhiko Morita, Masanori Kishimoto, and Takami Tohyama, “Ground-state phase diagram of the kitaev-heisenberg model on a kagome lattice,” *Phys. Rev. B* **98**, 134437 (2018).
 - 27 Yang Yang, Natalia B. Perkins, Fulya Koç, Chi-Huei Lin, and Ioannis Rousochatzakis, “Quantum-classical crossover in the spin- $\frac{1}{2}$ heisenberg-kitaev kagome magnet,” *Phys. Rev. Research* **2**, 033217 (2020).
 - 28 T. Holstein and H. Primakoff, “Field dependence of the intrinsic domain magnetization of a ferromagnet,” *Phys. Rev.* **58**, 1098–1113 (1940).
 - 29 M. Z. Hasan and C. L. Kane, “Colloquium: Topological insulators,” *Rev. Mod. Phys.* **82**, 3045–3067 (2010).
 - 30 Xiao-Liang Qi and Shou-Cheng Zhang, “Topological insulators and superconductors,” *Rev. Mod. Phys.* **83**, 1057–1110 (2011).
 - 31 Di Xiao, Ming-Che Chang, and Qian Niu, “Berry phase effects on electronic properties,” *Rev. Mod. Phys.* **82**, 1959–2007 (2010).
 - 32 Yasuhiro Hatsugai, “Chern number and edge states in the integer quantum hall effect,” *Phys. Rev. Lett.* **71**, 3697–3700 (1993).
 - 33 Ryo Matsumoto and Shuichi Murakami, “Theoretical prediction of a rotating magnon wave packet in ferromagnets,” *Phys. Rev. Lett.* **106**, 197202 (2011).
 - 34 Ryo Matsumoto and Shuichi Murakami, “Rotational motion of magnons and the thermal hall effect,” *Phys. Rev. B* **84**, 184406 (2011).
 - 35 Ryo Matsumoto, Ryuichi Shindou, and Shuichi Murakami, “Thermal hall effect of magnons in magnets with dipolar interaction,” *Phys. Rev. B* **89**, 054420 (2014).